THE JOURNAL OF PHYSICAL CHEMISTRY B

Article

pubs.acs.org/JPCB

On the Morphology of Viral Capsids: Elastic Properties and Buckling Transitions

Eric R. May and Charles L. Brooks, III*

Department of Chemistry and Biophysics Program, University of Michigan, Ann Arbor, Michigan 48109, United States

ABSTRACT: The morphology of icosahedral viruses ranges from highly spherical to highly faceted, and for some viruses a shape transition occurs during the viral life cycle. This phenomena is predicted from continuum elasticity, via the buckling transition theory by Nelson (*Phys. Rev. E* **2003**, *68*, 051910), in which the shape is dependent on the Foppl−von Kármán number (γ), which is a ratio of the two-dimensional Young's modulus (Y) and the bending modulus (κ). However, until now, no direct calculations have been performed on atomic-level capsid structures to test the predictions of the theory. In this study, we employ a previously described multiscale method by May and Brooks (*Phys. Rev. Lett.* **2011**, *106*, 188101) to calculate Y and κ for the bacteriophage HK97, which undergoes a spherical to faceted transition during its viral life cycle. We observe a change in γ consistent with the buckling transition theory and also a significant reduction in κ, which facilitates formation of the faceted state. We go on to examine many capsids from the $T = 3$ and 7 classes using only elastic network models, which allows us to calculate the ratio Y/κ, without the expense of all-atom molecular dynamics. We observe for the $T = 7$ capsids, there is strong correlation between the shape of the capsid and γ; however, there is no such correlation for the smaller $T = 3$ viruses.

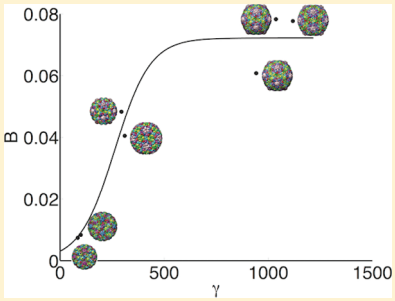

INTRODUCTION

Understanding the physical principles that govern virus equilibrium and dynamical properties is of great importance for improving antiviral therapies and also for using virus-based protein shells in nanotechnology applications.[1] The simplest and structurally best characterized classes of viruses are the spherical viruses, which, in the most basic cases, consist of only nucleic acid, surrounded by a protein shell (capsid).[2,3] The capsids of spherical viruses are built from a single (or a small number of) protein subunit copied 60T times. The subunits are arranged to reflect icosahedral (60-fold) symmetry and are classified by their triangulation number, T. The T number indicates how many subunits make up the asymmetric unit,[4,5] which is the smallest unique structural element in icosahedral capsids. The structure of the capsids reveals that the proteins pack into five-member (pentamer) and six-member (hexamer) aggregates, collectively know as capsomers. The ability of the proteins to pack into different symmetry environments is known as the principle of quasi-equivalence.[5] All spherical capsids consist of 12 pentmers and a variable number of hexamers, which allows for a highly scalable design.[6,7]

In addition to a wide range of sizes, spherical viruses exhibit a range of shapes. While some viruses exhibit "rough" surfaces with protruding domains, others are very geometrical, ranging from highly spherical to more polyhedral (icosahedral), displaying sharp angles and flat faces. Figure 1 demonstrates the shape and size diversity in two capsid classes, $T = 3$ and 7. In one well-studied system, the bacteriophage HK97, a spherical to faceted shape transition occurs during the viral life cycle, coinciding with the particle transforming from a noninfectious (immature) to an infectious (mature) particle.[8−10] The maturation process of HK97 is believed to share many commonalities with other double-stranded (ds)DNA bacteriophages, as well as herpes virus.[8,10] Hence, understanding the determinants of capsid morphology is enlightening to not only the equilibrium shapes that capsids adopt but also dynamical viral processes.

The life cycle of HK97 involves the formation of an immature capsid, prohead II (Figure 1, bottom row, third from right), which is smaller and rounded compared to the mature head II structure (Figure 1, bottom row, third from left). The in vivo maturation of HK97 is triggered by the packaging of the dsDNA genome through a portal at one of the pentameric sites. The packaging of DNA exerts a very large pressure (~50 atm) on bacteriophage capsids, as measured in optical tweezer pulling experiments.[11,12] HK97 maturation involves morphological changes to the capsid, configurational changes to the subunit proteins, and also a chemical change in the form of isopeptide bond formation (cross-links) between residue side chains (Lys169-Asn356) on neighboring subunits, leading to a unique protein catenane topology.[8]

One might assume the mechanical pressure from the DNA is the driving force for expansion and that the cross-links act to "pull" the capsid along the expansion pathway and stabilize the expanded capsid, while the capsid proteins act as passive members in the maturation theatrics. However, there are several in vitro experiments that refute this view and point

Special Issue: Macromolecular Systems Understood through Multiscale and Enhanced Sampling Techniques

Received: January 1, 2012
Revised: March 7, 2012
Published: March 12, 2012

   dx.doi.org/10.1021/jp300005g | *J. Phys. Chem. B* 2012, 116, 8604−8609

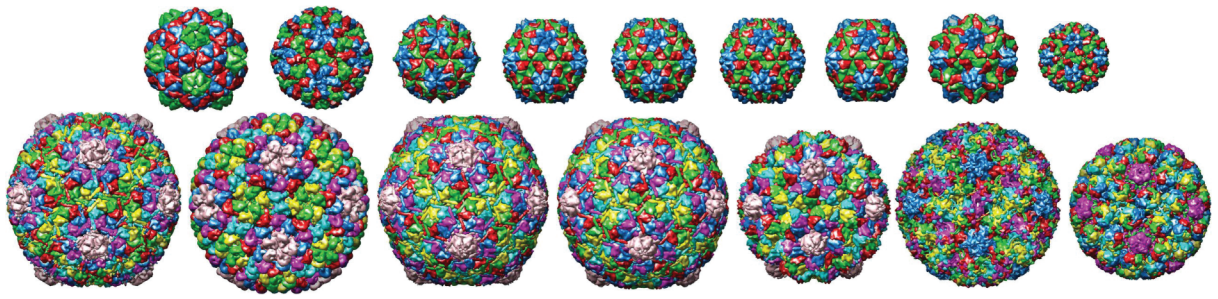

Figure 1. A sampling of spherical capsids, VIPERdb code in parentheses. T = 3 capsids (top row, l to r): Virus-like particle from *Pyrococcus furious* (2e0z), norwalk virus (1ihm), flockhouse virus (2z2q), southern bean mosaic virus (4sbv), sesbania mosaic virus (1smv), cocksfoot mottle virus (1 ng0), tobacco necrosis virus (1c8n), and cowpea chlorotic mottle virus (1cwp). T = 7 capsids (bottom row, l to r): ε15 (3c5b), p22 (2xyy), HK97 head II (1ohg), HK97 head I (2fs3), HK97 prohead II (3e8k), bovine papilloma virus (3iyj), and simian virus 40 (1sva).

toward the subunits as active players in modulating the morphology of the capsid. The first evidence comes from the fact that portal deficient capsids can be matured in the absence of DNA, the trigger in this case being exposure to a low-pH environment (pH ≈ 4).[13,14] Second, the expansion process can occur in the absence of cross-link formation, which was demonstrated for a cross-link deficient mutant (K169Y).[15] In this mutant particle, the maturation results in a structure highly similar to head II, know as head I, shown in Figure 1, bottom row, center. The ability for the particle to expand and facet in the absence of DNA and the inability to cross-link leads to the notion of a spontaneous mechanism whereby the properties of the proteins are altered in differing electrostatic environments (low pH), which triggers a change to the mature configuration.

Two notable explanations have emerged to account for the observed shape diversity in capsids, one rooted in continuum elasticity[16] and the other in geometry.[6] Lidmar, Minry, and Nelson (LMN) put forth the buckling transition of spherical shells[16] as an extension of the theory describing buckling of flat plates,[17] in which the pentamers are viewed as a five-fold disclination in a hexagonal lattice. This pentameric disclination introduces a strain that can be relieved by the pentamer buckling out-of-plane (forming a faceted shape); however, this introduces a bending strain to the system. The buckling transition theory envisions a competition between in-plane and out-of-plane strain energies, which can be quantified in terms of the two-dimensional Young's modulus (Y) and the bending modulus (κ), respectively. A single parameter, the Foppl−von Kármán number, $\gamma = YR^2/\kappa$, is a predictor of if the shell buckles, where R is the shell radius. The buckling of flat plates was shown to occur at $\gamma_B \geq 154$,[17] γ_B being the critical buckling value, and LMN observed deviations from spherical shapes for shells with values of $\gamma > 154$. Nguyen, Bruinsma, and Gelbart (NBG) performed a subsequent study to examine the effects of nonzero spontaneous curvatures on the elasticity and shapes of shells.[18] In the NBG study, they performed numerical energy minimization of shells, and in the case of zero spontaneous curvature, they found $\gamma_B = 260$. (NBG defines $\gamma = YS/\kappa$, where S is the surface area of the shell. NBG calculated $\gamma_B = 3269$; by taking $S = 4\pi R^2$, one can arrive at $\gamma_B = 260$.) While the origin of the different γ_B values between LMN and NBG was not identified, these are reasonably close values, and we will reference the NBG value throughout this paper. The geometrical theory of Mannige and Brooks[7,19] posits that a given T number capsid has a distinct set of hexamer shapes available, based on the constraints imposed by the pentameric angles. In the case of T = 7 capsids, only a single hexamer shape exists, but this hexamer has a single degree of freedom that allows for radial dimpling of the hexamer, which they consider analogous to buckling. While these viewpoints might be mutually compatible, we will focus on exploring the buckling transition theory of Nelson by employing calculations on atomically detailed capsid structures (as opposed to toy models).

The elastic properties of virus capsids have been explored primarily through atomic force microscopy (AFM) nano-indentation[20−25] and computational modeling studies.[26−32] While there is some variability between virus systems, in large, it has been shown that capsids are deformable and display a linear elastic response. Repeated indentations can lead to fatigue and plastic deformations, and large indentations will permanently fracture the capsid. The experimental studies can measure a bulk spring constant, which can be related to a three-dimensional Young's modulus (E), while we have developed a multiscale computational method that allows for calculation of Y and κ from equilibrium molecular simulations.[31] We also have shown that the magnitude of fluctuations along a single spherical harmonic mode (l = 1) at equilibrium provides a good estimate of the stiffness sensed in AFM-induced deformations.[30] Recently, a combined experimental and theoretical study on the effects of maturation on the mechanical properties of HK97 was performed.[33] The modeling and experiments agreed in predicting a significant increase in E due to maturation. The study went on to examine the role of cross-linking in strengthening the capsid, and it was shown that cross-links are not the only factor influencing the mechanical properties. The experiments showed that an intermediate structure with a low-level of cross-linking had the same critical force (force required to break the capsid) as the fully cross-linked head II particle, while the simulations showed that the mature particle without cross-links (head I) displayed nearly the same E value as head II. These interesting findings point toward the topological rearrangement and tertiary contacts of the capsid proteins as an important component of the mechanical stability of the mature capsids.

In this study, we explore the link between the morphology and two-dimensional elastic properties of capsids, à la, the buckling transition theory. We revisit HK97 using the multiscale approach, focusing on the prohead II and head I structures, to elucidate how protein configurational changes alone (without cross-linking) can influence the elastic properties. The multiscale calculation involves simulations of the entire capsid using an (inexpensive) elastic network model (ENM) and (expensive) all-atom molecular dynamics (MD) of

dx.doi.org/10.1021/jp300005g | J. Phys. Chem. B 2012, 116, 8604−8609

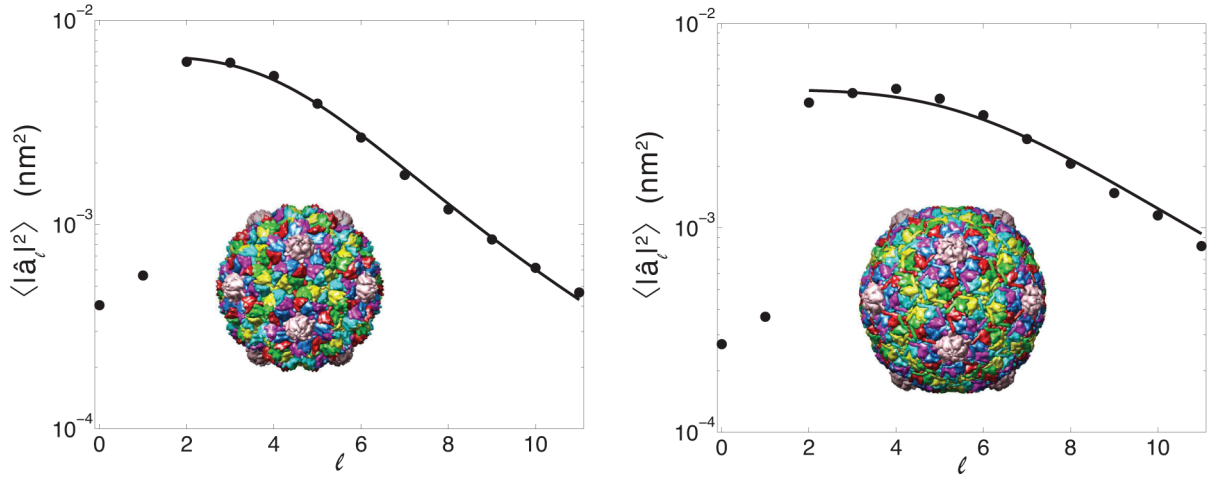

Figure 2. Equilibrium fluctuation spectrum projected on the spherical harmonic basis for HK97 in prohead II (left) and head I (right) configurations; PDB structures are shown on insets (prohead II: 3e8k; head I: 2fs3).

the seven-protein asymmetric unit. The all-atom MD allows us to renormalize the ENM simulation such that we can obtain quantitative estimates of Y and κ. However, the ENM calculation alone allows the ratio Y/κ and hence γ to be determined. We employ this less-expensive method on a series of capsids from the $T = 3$ and 7 classes, which provide a large enough sample to detect correlations between the capsid shape and elastic behavior.

METHODS

The capsid structures were downloaded from the VIPERdb site;[3] all structures were high-resolution (<5.0 Å). All structures contained backbone and side-chain heavy atoms, except for p22 and ε15, which only contained Cα atoms. For our study of HK97, we employed a multiscale approach to generate the equilibrium capsid dynamics representative of a particular temperature.[31] The method involves the construction of an ENM, propogatation of the network along the lowest-frequency normal modes, and a renormalization procedure to ensure that our ENM spectrum is scaled to the appropriate thermal scale. To renormalize the fluctuations in the ENM dynamics, we computed a MD trajectory of the capsid asymmetric unit under icosahedral boundary conditions[34] using the CHARMM simulation package and CHARMM19 force field.[35,36] The initial configurations of the asymmetric units were energy-minimized and then equilibrated at 300 K with an Andersen thermostat using the GBSW implicit solvent model.[37] The systems were equilibrated for 10 ns followed by production simulations for 10 ns. The dynamics were computed with a 2 fs time step, and the trajectories were saved every 1000 steps (every 2 ps) for analysis.

The ENM models consisted of all heavy atoms and were constructed by imposing the icosahedral rotations on the average structure of the asymmetric unit from the production MD simulations, to build a complete capsid. Harmonic bonds were placed between atoms separated by 5 Å or less, and the rotation−translation of blocks (RTB) method[38] was used to diagonalize the Hessian matrix of the potential energy and determine the normal modes of the network. In this method, segments of the structure are treated as rigid units; we chose to make two consecutive residues a rigid unit in our analysis. The networks were propagated along the 999 lowest-frequency modes (excluding the first 6 modes, which correspond to rigid body motions) to construct a trajectory long enough to observe ∼20 oscillations of the slowest modes.

The dynamics from the ENM are decomposed by first computing the capsid surface by binning atoms on an equiangular grid. All surfaces were computed on a grid with 24 grid points in both the polar and azimuthal directions, for a total of 576 grid points. The positions of the surface are given by the average radial position of all heavy atoms falling into each bin (non-mass-weighted). A spherical harmonic decomposition is then preformed using the SpharmonicKit software package.[39] The dynamics from the MD simulation are also decomposed by first constructing a complete capsid at each frame in the trajectory by imposing the icosahedral operations. The complete capsid dynamics from MD are decomposed in the same manner as the ENM dynamics. The magnitude of the MD equilibrium fluctuations were calculated by performing block averaging over 4 ns blocks of data; the blocks were offset by 1 ns, for a total of seven blocks. The scaling factor from MD for prohead II and head I were $(3.02 \pm 0.38) \times 10^{-2}$ and $(2.99 \pm 0.44) \times 10^{-2}$ nm^2, respectively. The spherical harmonic coefficients from the ENM $\langle |\hat{a}_l|^2 \rangle_{\mathrm{ENM}}$ are renormalized by the MD coefficients according to

$$\langle |\hat{a}_l|^2 \rangle^{\#}_{\mathrm{ENM}} = \left(\frac{\sum_l \langle |\hat{a}_l|^2 \rangle_{\mathrm{MD}}}{\sum_l \langle |\hat{a}_l|^2 \rangle_{\mathrm{ENM}}} \right) \langle |\hat{a}_l|^2 \rangle_{\mathrm{ENM}} \quad (1)$$

where # indicates the renormalized values. This renormalization has the effect of conserving the sum of the mode magnitudes between the MD and ENM systems, which is a representation of the system temperature according to our elastic model (see eq 2).

For the calculations in which we only employed ENMs, the ENMs were constructed and propagated in the same manner as the multiscale approach with a few adjustments. The structures used to construct the network were the structures downloaded from VIPERdb, and the networks were built from all-heavy atoms, unless the structure only contained Cα positions. The cutoff distance for determining bonds in the network was 5 Å for all systems except those in which only Cα atoms were present in the structure; for those Cα structures, a 12 Å cutoff was used. Also, for all systems except p22, five consecutive residues were treated as a rigid block in the RTB method; for p22, six consecutive residues comprised a block.

dx.doi.org/10.1021/jp300005g | J. Phys. Chem. B 2012, 116, 8604−8609

Table 1. Comparison of Structural and Elastic Properties of Capsids

virus	family	T#	R (nm)	h (nm)	B	Y/κ (nm^{-2})	γ
cowpea chlorotic mottle virus	bromoviridae	3	11.8	2.9	0.027	0.43	60
turnip yellow mosaic virus	tymoviridae	3	12.7	2.6	0.043	0.59	95
tobacco necrosis virus	tombusviridae	3	12.9	2.5	0.067	0.89	148
cocksfoot mottle virus	sobemoviridae	3	13.0	2.7	0.066	0.72	122
sesbania mosaic virus	sobemoviridae	3	13.0	2.6	0.059	0.92	156
southern bean mosiac virus	sobemoviridae	3	13.1	2.7	0.059	0.83	141
flockhouse virus	nodaviridae	3	13.7	4.3	0.064	0.33	62
norwalk virus	caliciviridae	3	15.8	6.2	0.021	0.19	48
VLP from *Pyrococcus furiosus*	n/a	3	16.2	2.6	0.035	0.91	238
simian virus 40	polyomaviridae	7*d*	21.2	5.3	0.007	0.19	84
HK97 prohead II	siphoviridae	7*l*	23.0	4.0	0.048	0.56	294
bovine papilloma virus	papillomaviridae	7*d*	24.5	6.3	0.008	0.17	99
p22	podoviridae	7*l*	26.6	4.0	0.040	0.44	311
HK97 head I	siphoviridae	7*l*	27.9	2.7	0.061	1.21	942
HK97 head II	siphoviridae	7*l*	28.2	2.7	0.078	1.30	1036
ϵ15	podoviridae	7*l*	28.9	2.4	0.078	1.34	1118

RESULTS AND DISCUSSION

We begin by computing the equilibrium fluctuation spectrum of HK97 in the prohead II and head I states, using our multiscale approach,[31] to explore the relationship between morphological changes (maturation) and elastic properties. The spectra are shown in Figure 2, and it can be observed that the $l \geq 2$ modes are well-described by an elastic model equation, in which normal displacements are decomposed in a spherical harmonic basis[31,40]

$$\langle |\hat{a}_l|^2 \rangle = \frac{k_B T}{8b + \kappa \frac{l(l-1)(l+1)(l+2)}{R^2}} \quad (2)$$

where b is the sum of the Lamé constants, $(\lambda + \mu)$, $|\hat{a}_l|^2 \equiv \sum_{m=-l}^{+l} a_{lm} a_{lm}^*$, a_{lm} is the magnitude of the spherical harmonic Y_{lm}, * indicates the complex conjugate, and k_B is the Boltzmann constant. By fitting eq 2 to the spectra, we can calculate the parameters, b and κ. By choosing a value for the Poisson ratio, σ, we can calculate Y from b;[31,41,42] we choose $\sigma = 0.3$.[29]

From our fits in Figure 2, we calculate for prohead II, $\kappa = 57 k_B T$, $Y = 26 k_B T/nm^2$, and $\gamma = 207$, and for head I, we calculate $\kappa = 30 k_B T$, $Y = 37 k_B T/nm^2$, and $\gamma = 742$. The change in γ is consistent with the buckling transition theory in that the spherical prohead II state lies below the critical value ($\gamma_B = 260$) while the faceted head I state is well above the critical value. While the change in radius from 21 nm in the prohead II state to 24 nm in the head I state accounts for much of the change in γ, there are also significant changes in the elastic properties. Y increases significantly during the transition, while κ is nearly halved during the transition. Both of the changes are functionally sensible; the increase in Y indicates a stabilization of the capsid, which may act to resist the pressure from an encapsidated genome. The decrease in κ allows for the faceted structure, which has regions of high curvature, to be adopted at a lower bending energy cost to the system. The ratio Y/κ increases from 0.46 to 1.23 nm^{-2} during the transition, which is consistent with thin shell theory, which states $Y = Eh$ and $\kappa = Eh^3/[12(1 - \sigma^2)]$, where h is the thickness of the shell and E is the three-dimensional Young's modulus.[41] The thickness of the shell decreases from 3.83 to 2.69 nm during the transition; therefore (if thin shell theory holds)

$$\frac{(Y/\kappa)_{\text{prohead II}}}{(Y/\kappa)_{\text{head I}}} = \left(\frac{h_{\text{head I}}}{h_{\text{prohead II}}} \right)^2 \quad (3)$$

and indeed, the ratio of elastic properties is 0.38, which is close to the squared thickness ratio of 0.49.

Our calculations support the modulation of elastic properties as a valid mechanism to drive the morphological changes associated with HK97 maturation. To extend this, we would like to understand, in general, if γ is a good predictor of observed capsid shapes. While our multiscale approach allows us to quantitatively estimate the properties κ and Y, there is significant computational expense associated with the MD simulations of the asymmetric units. However, we can estimate the ratio Y/κ and γ without the MD simulation and rely only on our normal-mode-based ENM trajectories. We have taken this approach to study a sampling of capsids from the $T = 7$ and 3 classes. The capsid structures studied are shown in Figure 1, and the calculated structural and elastic properties are presented in Table 1. Our sample of capsids consists of 16 structures, from 10 virus families and 1 nonviral structure, a virus-like particle (VLP) from *Pyrococcus furiosus* archaea.

To characterize the degree of faceting/buckling, we define a buckling parameter[43]

$$B = \frac{1}{R} \left(\frac{1}{N_{\text{pent}}} \sum_{i=1}^{N_{\text{pent}}} r_{i,\text{pent}} - \frac{1}{N_{\text{hex}}} \sum_{i=1}^{N_{\text{hex}}} r_{i,\text{hex}} \right) \quad (4)$$

where N_{pent} and N_{hex} are the numbers of pentameric and hexameric atoms, respectively, $r_{i,\text{pent(hex)}}$ is the radial position of the ith pentameric (hexameric) atom, and R is the mean capsid radius; the calculation is performed with the center of geometry of the capsid placed at the origin. B serves to measure the degree to which the pentamers extend radially away from the hexamers and is normalized by the capsid radius, such that capsids of different sizes and T numbers may be compared. In the sample of capsids that we study, B spans a full order of magnitude from 0.007 to 0.078, while the ratio of elastic properties, Y/κ, also displays nearly one order of magnitude variation (0.17−1.34 nm^{-2}).

dx.doi.org/10.1021/jp300005g | J. Phys. Chem. B 2012, 116, 8604−8609

When we examine the relationship between B and γ (Figure 3), we observe that the $T = 3$ capsids display a significant

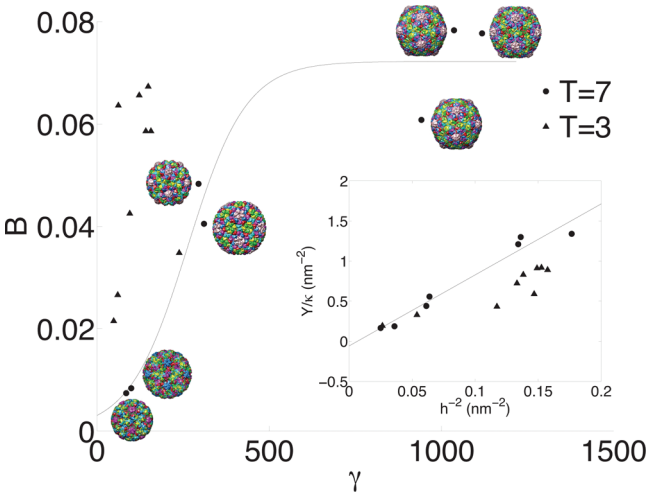

Figure 3. Relationship between the shape and γ. The $T = 7$ capsids are fit by a sigmoidal function, and the capsid structures are shown next to each of the corresponding data points. (Inset) Y/κ is plotted against h^{-2}, and a linear regression is fit to the $T = 7$ data points.

variation in B, with minimal variation in γ. However, the $T = 7$ capsids do appear to be correlated with γ. We fit the $T = 7$ data by a sigmodial functional form, $f(x) = A/(1 + \exp(-B(x - C))$, which provides a good fit to the data. The curve has an inflection point at $x = C$, and from the fit, we obtain $C = 263$. The inflection value of $\gamma = 263$ is remarkably close to the expected critical buckling value $\gamma_B = 260$.[18] In the inset of Figure 3, we examine the thin shell approximation by plotting Y/κ against h^{-2} and observe a linear relationship. The thin shell equations predict a slope of $12(1 - \sigma^2)$,[41] which, for our choice of $\sigma = 0.3$, yields 10.9; by fitting a first-order polynomial to all of the $T = 7$ data, we obtain a slope of 8.9 (shown in Figure 3, inset), in reasonable agreement with the thin shell theory. However, if the fit is performed on the $T = 3$ data points, the slope is 5.2, which significantly departs from the predicted thin shell theory estimate.

CONCLUSIONS

For the first time, we have tested the predictions of the buckling transition theory[16,18] by calculating the elastic properties of atomically detailed capsid structures on a sample of capsids that display a range of morphologies. We have found that the maturation transition of HK97 can be characterized as a buckling transition, based on our calculation that γ crosses the critical buckling value during the maturation process. The change in γ is not entirely due to radial expansion but also due to significant changes in Y and κ. The changes in the elastic properties are functionally relevant in that the increase in Y will stabilize the capsid against internal and external pressures and the reduction in κ will facilitate formation of high-curvature regions of the faceted configuration. The ratios of Y/κ in the prohead II and head I states are consistent with the thin shell theory predictions.

We have shown that the $T = 7$ capsids show a strong correlation between γ and the degree of buckling, B, while the $T = 3$ capsids do not. Remarkably, the critical buckling value, γ_B, predicted from theory is nearly identical to the value that we calculate by fitting a sigmoidal curve to the $T = 7$ data. The fact that the $T = 3$ structures do not show a correlation between γ and B consistent with that of a buckling transition is likely due to the breakdown in the continuum elasticity approximations. The h/R ratios are much larger for the $T = 3$ shells, and the relationship between Y/κ and h shows significant deviations from the thin shell theory predictions, indicating that two-dimensional elasticity theory is insufficient. The $T = 3$ structures are possibly in a molecular-mechanics-dominated regime, while the larger $T = 7$ are in the continuum-mechanics-dominated regime. Viruses larger than $T = 7$ become more complex often due to the auxiliary and scaffolding protein required to stabilize the capsid. Nonetheless, larger viruses generally do adopt more faceted configurations, and we would expect them to have large γ values due to their large radius and given that Y/κ is likely to remain relatively close to 1 nm^{-2}.

We hope that these findings will be impactful for nanotechnology design, in which controlling and manipulating the size/shape of protein containers is a critical component in the design of these devices. We believe that it is a significant and interesting finding that capsids do display a range of magnitudes in their elastic properties, and a single system can modulate these properties to facilitate shape changes. The next step in gaining a more complete picture of how these changes are manifested is to try to identify critical interactions that are broken (formed) by exposure to differing electrostatic/pH environments and also how the elastic properties change as a system progresses from one state to another; we are currently undertaking such studies.

AUTHOR INFORMATION

Corresponding Author

*E-mail: brookscl@umich.edu. Phone: (734)647-6682. Fax: (734)647-1604.

Notes

The authors declare no competing financial interest.

ACKNOWLEDGMENTS

This work has been supported by the Center for Theoretical Biological Physics through the NSF (PHY-0216576) and is also supported by the NIH to C.L.B. (RR012255), the NSF to C.L.B. (MCB-1121575), and by the NSF to E.R.M. (DBI-0905773).

REFERENCES

(1) *Viruses and Nanotechnology*; Manchester, M., Steinmetz, N. F., Eds.; Springer-Verlag: New York, 2009; Vol. *327*

(2) *Structural Biology of Viruses*; Chiu, W., Burnett, R., Garcea, R., Eds.; Oxford University Press: New York, 1997.

(3) Carrillo-Tripp, M.; Shepherd, C. M.; Borelli, I. A.; Venkataraman, S.; Lander, G.; Natarajan, P.; Johnson, J. E.; Brooks, C. L. III; Reddy, V. S. *Nucleic Acids Res.* **2009**, *37*, D436−D442.

(4) Crick, F. H.; Watson, J. D. *Nature* **1956**, *177*, 473−475.

(5) Caspar, D. L.; Klug, A. *Cold Spring Harbor Symp. Quant. Biol.* **1962**, *27*, 1−24.

(6) Mannige, R. V.; Brooks, C. L. III. *Phys. Rev. E* **2008**, *77*, 051902.

(7) Mannige, R. V.; Brooks, C. L. III. *Proc. Natl. Acad. Sci. U.S.A.* **2009**, *106*, 8531−8536.

(8) Wikoff, W. R.; Liljas, L.; Duda, R. L.; Tsuruta, H.; Hendrix, R. W.; Johnson, J. E. *Science* **2000**, *289*, 2129−2133.

(9) Conway, J. F.; Wikoff, W. R.; Cheng, N.; Duda, R. L.; Hendrix, R. W.; Johnson, J. E.; Steven, A. C. *Science* **2001**, *292*, 744−748.

(10) Gertsman, I.; Gan, L.; Guttman, M.; Lee, K.; Speir, J. A.; Duda, R. L.; Hendrix, R. W.; Komives, E. A.; Johnson, J. E. *Nature* **2009**, *458*, 646−650.

(11) Smith, D. E.; Tans, S. J.; Smith, S. B.; Grimes, S.; Anderson, D. L.; Bustamante, C. *Nature* **2001**, *413*, 748−752.
(12) Tzlil, S.; Kindt, J. T.; Gelbart, W. M.; Ben-Shaul, A. *Biophys. J.* **2003**, *84*, 1616−1627.
(13) Duda, R. L.; Hempel, J.; Michel, H.; Shabanowitz, J.; Hunt, D.; Hendrix, R. W. *J. Mol. Biol.* **1995**, *247*, 618−635.
(14) Lata, R.; Conway, J. F.; Cheng, N.; Duda, R. L.; Hendrix, R. W.; Wikoff, W. R.; Johnson, J. E.; Tsuruta, H.; Steven, A. C. *Cell* **2000**, *100*, 253−263.
(15) Conway, J. F.; Duda, R. L.; Cheng, N.; Hendrix, R. W.; Steven, A. C. *J. Mol. Biol.* **1995**, *253*, 86−99.
(16) Lidmar, J.; Mirny, L.; Nelson, D. R. *Phys. Rev. E* **2003**, *68*, 051910.
(17) Seung, H. S.; Nelson, D. R. *Phys. Rev. A* **1988**, *38*, 1005−1018.
(18) Nguyen, T. T.; Bruinsma, R. F.; Gelbart, W. M. *Phys. Rev. E* **2005**, *72*, 051923.
(19) Mannige, R. V.; Brooks, C. L. III. *PLoS One* **2010**, *5*, e9423.
(20) Ivanovska, I. L.; de Pablo, P. J.; Ibarra, B.; Sgalari, G.; MacKintosh, F. C.; Carrascosa, J. L.; Schmidt, C. F.; Wuite, G. J. L. *Proc. Natl. Acad. Sci. U.S.A.* **2004**, *101*, 7600−7605.
(21) Michel, J. P.; Ivanovska, I. L.; Gibbons, M. M.; Klug, W. S.; Knobler, C. M.; Wuite, G. J. L.; Schmidt, C. F. *Proc. Natl. Acad. Sci. U.S.A.* **2006**, *103*, 6184−6189.
(22) Kol, N.; Gladnikoff, M.; Barlam, D.; Shneck, R. Z.; Rein, A.; Rousso, I. *Biophys. J.* **2006**, *91*, 767−774.
(23) Roos, W. H.; Bruinsma, R.; Wuite, G. J. L. *Nat. Phys.* **2010**, *6*, 733−743.
(24) Roos, W. H.; Gibbons, M. M.; Arkhipov, A.; Uetrecht, C.; Watts, N. R.; Wingfield, P. T.; Steven, A. C.; Heck, A. J. R.; Schulten, K.; Klug, W. S.; et al. *Biophys. J.* **2010**, *99*, 1175−1181.
(25) Ivanovska, I. L.; Miranda, R.; Carrascosa, J. L.; Wuite, G. J. L.; Schmidt, C. F. *Proc. Natl. Acad. Sci. U.S.A.* **2011**, *108*, 12611−12616.
(26) Klug, W. S.; Bruinsma, R. F.; Michel, J.-P.; Knobler, C. M.; Ivanovska, I. L.; Schmidt, C. F.; Wuite, G. J. L. *Phys. Rev. Lett.* **2006**, *97*, 228101.
(27) Arkhipov, A.; Roos, W. H.; Wuite, G. J. L.; Schulten, K. *Biophys. J.* **2009**, *97*, 2061−2069.
(28) Zink, M.; Grubmüller, H. *Biophys. J.* **2009**, *96*, 1350−1363.
(29) Yang, Z.; Bahar, I.; Widom, M. *Biophys. J.* **2009**, *96*, 4438−4448.
(30) May, E. R.; Aggarwal, A.; Klug, W. S.; Brooks, C. L. III. *Biophys. J.* **2011**, *100*, L59−L61.
(31) May, E. R.; Brooks, C. L. III. *Phys. Rev. Lett.* **2011**, *106*, 188101.
(32) May, E.; Arora, K.; Mannige, R.; Nguyen, H.; Brooks, C. L., III In *Computational Modeling of Biological Systems: From Molecules to Pathways*; Dokholyan, N., Ed.; Springer-Verlag: New York, 2011; Chapter Multiscale Approaches to Studying Virus Structure, Assembly and Dynamics.
(33) Roos, W. H.; Gertsman, I.; May, E. R.; Brooks, C. L. III; Johnson, J. E.; Wuite, G. J. L. *Proc. Natl. Acad. Sci. U.S.A.* **2012**, *109*, 2342−2347.
(34) Cagin, T.; Holder, M.; Pettitt, B. *J. Comput. Chem.* **1991**, *12*, 627−634.
(35) Brooks, B. R.; Bruccoleri, R. E.; Olafson, B. D.; States, D. J.; Swaminathan, S.; Karplus, M. *J. Comput. Chem.* **1983**, *4*, 187−217.
(36) Brooks, B. R.; Brooks, C. L. III; Mackerall, A. D. Jr.; Nilsoon, L.; Petrella, R. J.; Roux, B.; Won, Y.; Archontis, G.; Bartels, C.; Boresh, S.; et al. *J. Comput. Chem.* **2009**, *30*, 1545−1614.
(37) Im, W.; Lee, M. S.; Brooks, C. L. III. *J. Comput. Chem.* **2003**, *24*, 1691−1702.
(38) Tama, F.; Gadea, F. X.; Marques, O.; Sanejouand, Y. H. *Proteins* **2000**, *41*, 1−7.
(39) Healy, D. M.; Rockmore, D. N.; Kostelec, P. J.; Moore, S. *J. Fourier Anal. Appl.* **2003**, *9*, 341−385.
(40) Widom, M.; Lidmar, J.; Nelson, D. R. *Phys. Rev. E* **2007**, *76*, 031911.
(41) Landau, L.; Lifshitz, E. *Theory of Elasticity*; Pergamon Press: Elmsford, NY, 1959.
(42) Buenemann, M.; Lenz, P. *Phys. Rev. E* **2008**, *78*, 051924.
(43) May, E. R.; Feng, J.; Brooks, C. L. III. *Biophys. J.* **2012**, *102*, 606−612.